# Band gap and defect states of MgO thin films investigated using reflection electron energy loss spectroscopy

Cite as: AIP Advances **5**, 077167 (2015); https://doi.org/10.1063/1.4927547
Submitted: 10 February 2015 • Accepted: 15 July 2015 • Published Online: 24 July 2015

Sung Heo, Eunseog Cho, Hyung-Ik Lee, et al.

# Band gap and defect states of MgO thin films investigated using reflection electron energy loss spectroscopy

Sung Heo,[1,2] Eunseog Cho,[3] Hyung-Ik Lee,[1] Gyeong Su Park,[1]
Hee Jae Kang,[4] T. Nagatomi,[5] Pyungho Choi,[2] and Byoung-Deog Choi[2,a]
[1]*Analytical Engineering Group, Samsung Advanced Institute of Technology, 130, Samsung-ro, Yeongtong-gu, Suwon-si, Gyeonggi-do, S. Korea, 443-803*
[2]*College of Information and Communication Engineering, Sungkyunkwan University, Cheoncheon-dong 300, Jangan-gu, Suwon 440-746, S. Korea*
[3]*CAE Group, Samsung Advanced Institute of Technology, 130, Samsung-ro, Yeongtong-gu, Suwon-si, Gyeonggi-do, S. Korea, 443-803*
[4]*Department of Physics, Chungbuk National University, Cheongju, S. Korea*
[5]*Analysis & Simulation Center, Asahi Kasei Corporation, 2-1 Samejima, Fuji, Shizuoka 416-8501, Japan*

(Received 10 February 2015; accepted 15 July 2015; published online 24 July 2015)

The band gap and defect states of MgO thin films were investigated by using reflection electron energy loss spectroscopy (REELS) and high-energy resolution REELS (HR-REELS). HR-REELS with a primary electron energy of 0.3 keV revealed that the surface F center (FS) energy was located at approximately 4.2 eV above the valence band maximum (VBM) and the surface band gap width ($E_g^S$) was approximately 6.3 eV. The bulk F center ($F_B$) energy was located approximately 4.9 eV above the VBM and the bulk band gap width was about 7.8 eV, when measured by REELS with 3 keV primary electrons. From a first-principles calculation, we confirmed that the 4.2 eV and 4.9 eV peaks were $F_S$ and $F_B$, induced by oxygen vacancies. We also experimentally demonstrated that the HR-REELS peak height increases with increasing number of oxygen vacancies. Finally, we calculated the secondary electron emission yields (γ) for various noble gases. He and Ne were not influenced by the defect states owing to their higher ionization energies, but Ar, Kr, and Xe exhibited a stronger dependence on the defect states owing to their small ionization energies.  [http://dx.doi.org/10.1063/1.4927547]

## I. INTRODUCTION

MgO thin films have been used as a material to form a protective layer in alternating-current plasma display panels (AC-PDPs).[1–4] To display dynamic images using AC-PDPs, a firing voltage is applied to the electrodes to initiate discharge. Then, ultraviolet photons emitted from the plasma are absorbed in phosphors, and visible photons are generated. The protective MgO layer deposited on a glass dielectric in AC-PDPs plays an important role in protecting the dielectric layer from plasma damage. In addition, the MgO protective layer serves as a secondary electron emission layer, initiating the discharge.[5] Improving the performance of AC-PDPs and reducing the firing voltage of plasma (Vf) is essential, and can be achieved by using a protective layer with a higher ion-induced secondary electron (IISE) yield, γ. Therefore, γ is one of the most important parameters of the MgO protective layer for improving the discharge characteristics,[1,6] and the IISE phenomenon in MgO films has been intensively studied.[7–15] The magnitude of γ is strongly influenced by the MgO film electronic structure. It has been reported that γ is closely related to defect states[16] and γ increases as the number of surface defect states in MgO increases.[2] The defect states in MgO thin films consist

[a]E-mail: bdchoi@skku.edu

 

of bulk and surface defects, and the surface defect states affect γ much more strongly than the bulk defect states.[2]

The bulk defect states in MgO thin films have been studied by using photoluminescence (PL) and cathode luminescence (CL).[16,17] Rosenblatt *et al*. reported that F (oxygen ion vacancy) and F+ (oxygen ion vacancy + one electron) centers exist at 5 eV below the conduction band minimum of MgO.[17] Semi-empirical calculations revealed that F and F+ centers in MgO crystals are located at 3.0 and 2.96 eV above the valence band maximum (VBM), respectively.[18] Although the bulk defect states have been intensively studied, investigations of surface defect states have been very limited.

One of the most promising techniques for investigations of surface defect states is high-energy resolution reflective electron energy loss spectroscopy (HR-REELS) with a monochromatic electron gun, where a low primary energy of ~300 eV is employed, because its surface sensitivity is achieved by a shallow information depth. Wu *et al.*[11] investigated MgO thin films by using HR-REELS with primary electrons of 15 and 48 eV, at which the full width at half maximum (FWHM) of primary electrons was 50 meV. However, they were unable to explain the relationship between γ and the surface defect states of MgO.

In this study, we aimed to elucidate the relation between IISE and defect states in MgO films. To accomplish this, we investigated the surface defect states of MgO thin films by using HR-REELS with primary electron energy of 300 eV. We also studied the bulk defect states by using reflective electron energy loss spectroscopy (REELS) with primary electron energy of 3 keV, at which the FWHM of primary electrons was 0.8 eV. Using a first-principles calculation, we confirmed that the defect states originate at the F centers. Based on this calculation, we investigated the energies of the surface and bulk F centers, $F_S$ and $F_B$, respectively, and the surface and bulk band gap energies, $E_g^S$ and $E_g^B$, respectively. Furthermore, the values of γ for He+, Ne+, Ar+, Kr+, and Xe+ ions were calculated by using a model, reported by Motoyama *et al*.,[16] in which we used our first-principles calculation results on the density of states (DOS) to investigate the dependence of γ on the population of defects states.

## II. EXPERIMENTAL

The MgO thin film was deposited onto a p-type Si substrate (~100 Ω · cm) by electron beam evaporation, using MgO powder with 99.99% purity as an evaporation source. The base pressure in the deposition chamber was $2.0 \times 10^{-3}$ Pa and the substrate temperature during the deposition was 300 °C. The deposition rate of the MgO film was 0.8 nm/s and the film thickness was ~100 nm, controlled by the deposition time. After the deposition, the samples were annealed at 600 °C for 30, 60, and 90 min in an isolated ultra-high vacuum (UHV) chamber. The crystal structure of the MgO thin film, obtained by using X-ray diffraction (XRD), was a randomly oriented rock-salt structure.

The composition of the MgO thin film, and the bandgaps and energy levels of the defect states were measured by using Auger electron spectroscopy (AES; VG microlab 350 system). The primary energy of the electrons for the AES measurement was 0.3 keV with a monochromatic low-energy electron gun (VSW EM 50), and 3 keV with a normal electron gun. The FWHMs of the elastic peaks at 0.3 keV and 3 keV were 0.1 and 0.8 eV, respectively. HR-REELS at 0.3 keV and REELS at 3 keV were used for obtaining the surface- and bulk-sensitive band energy diagrams, respectively, because the inelastic mean free paths (IMFPs) of 0.3 and 3 keV electrons in MgO are 9.3 and 51.8 Å, respectively.[20]

The procedure for determining a band gap from a REELS spectrum is described elsewhere.[21]

## III. RESULTS AND DISCUSSION

Figure 1 shows the HR-REELS and REELS spectra obtained for the MgO thin film without any temperature treatment. The surface and bulk band gap values of the MgO thin film, $E_g^S$ = 6.3 eV and $E_g^B$ = 7.8 eV, were obtained from the threshold energy of the loss peak, as shown in Fig. 1. The value of $E_g^B$ was close to 7.77 eV, as reported by Roessler and Walker.[22] The obtained value of $E_g^S$

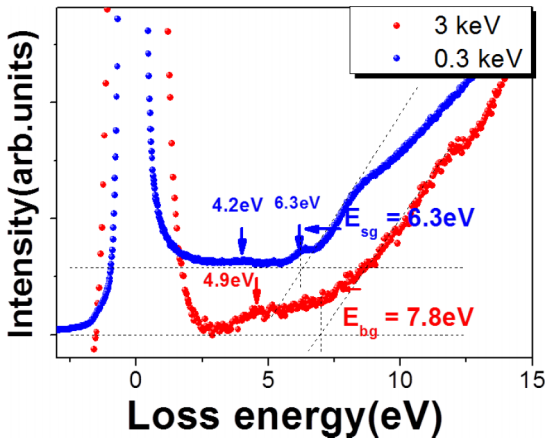


FIG. 1. REELS (red dots) and HR-REELS (blue dots) spectra obtained for the MgO film at the primary electron energies of 3 and 0.3 keV, respectively. No temperature treatment was performed before the measurement. The spectral intensity was normalized by the elastic peak height.

was in a good agreement with that reported by Henrich,[23] revealing that $E_g^S$ of the present MgO film without temperature treatment was 1.5 eV lower than $E_g^B$.

In the bulk-sensitive REELS spectrum at the primary energy of 3 keV, shown by red dots in Fig. 1, a small peak at 3.6 eV, attributed to the excitation of an electron from the surface F center to the conduction band minimum, corresponds to a state due to trapping of two electrons in an oxygen vacancy.[24] By contrast, the surface-sensitive HR-REELS spectrum shown by blue dots in Fig. 1 exhibits prominent loss peaks at 4.2 and 6.3 eV that are attributed to surface-localized excitation modes. It has been reported that the peak at 4.2 eV may be owing to the surface F center on the MgO surface.[25] The peak at 6.3 eV is related to the surface inter-band transition.[19] The energy level of the surface F center, $F_S$, is higher than that of the bulk F center, $F_B$.

To confirm the presence of defect states at 4.9 and 4.2 eV, a first-principles calculation was performed by utilizing the pseudo-potential plane wave method, using the Vienna ab-initio simulation package (VASP). With this package, we could not implement a computational method, supported by a new understanding of DFT,[26] which has been used to correctly describe and predict the band gaps in many semiconductors. This method minimizes the electron energy functional by using successfully larger basis sets. It is well known, from single basis set calculations, that the generalized gradient approximation (GGA) method usually gives a severely underestimated band gap value as compared to an experimentally obtained one. For example, the band gap of the bulk MgO calculated by using the GGA implemented by Perdew, Burke, and Ernzerhof (PBE) exchange-correlation energy functional is 5 eV,[27] which is only 64% of the experimentally measured band gap energy of 7.8 eV. Such an underestimation of the band gap energy makes a comparison between the calculated and measured energy levels of F centers difficult. Thus, in the present study, we have used a hybrid functional, the Heyd-Scuseria-Ernzerhof (HSE) exchange-correlation functional, with which 40% and 60% of the exchange energies are described as the Hatree-Fock and PBE exchange energies, respectively, with 100% of the PBE correlation energy. Using this approach, we obtained a bulk energy bandgap of 7.57 eV, which is 96% of the experimental value of 7.8 eV.

To calculate $E_g^B$, $E_g^S$, $F_B$, and $F_S$ with and without oxygen vacancies, we adopted both the MgO bulk structure and MgO(100) surface slab model. For the bulk structure, we built a $2 \times 2 \times 2$ supercell with $8 \times 8 \times 8$ k-point meshes, and one oxygen atom was eliminated from the supercell to mimic the bulk oxygen vacancy structure. For surface structure calculations, an MgO (100) surface model was built with $2 \times 2$ lateral symmetry and 9 layers slabs ($8 \times 8 \times 1$ k-points), as well as more than a 10-Å vacuum space in the slab direction, to prevent spurious interactions between the top and bottom atoms of the slabs through the supercells.

For modeling a surface with oxygen defects, we symmetrically eliminated two oxygen atoms on the top and the bottom layers to maintain a flat averaged local potential in the vacuum region by

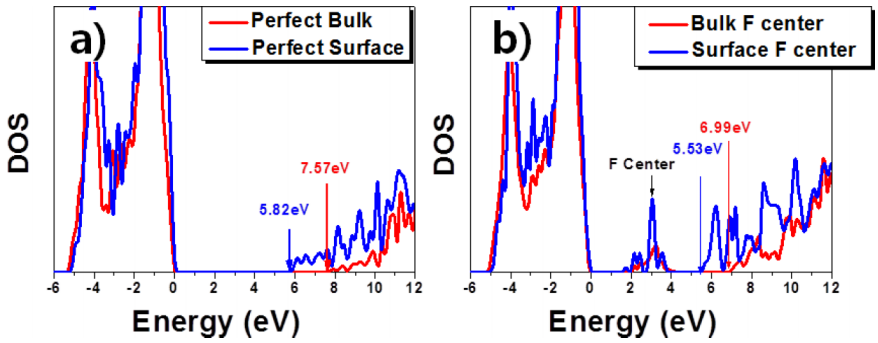


FIG. 2. Density of states (DOS) for (a) the perfect MgO (100) and (b) the F centers containing oxygen vacancies of 11 at% in the bulk and on the surface.

preventing the occurrence of unwanted dipole interactions. The energy cutoff was set to 400 eV and the atomic positions were fully relaxed until the Hellmann-Feynman force on each atom reached a value lower than 0.02 eV/Å.

Figure 2(a) shows the density of states (DOS) for the bulk and surface structures without oxygen vacancies. The obtained $E_g^B$ was 7.57 eV, corresponding to 96% of the experimental value. The calculated $E_g^S$ was 5.82 eV, lower than $E_g^B$ by 1.75 eV, which is in a good agreement with the experimental results in Fig. 1. From the results in Fig. 2(b), the values of $E_g^B$ and $E_g^S$ were 6.99 and 5.53 eV, respectively, and both were smaller than the corresponding ones obtained without oxygen vacancies.

The electronegativity of oxygen atoms is larger than that of magnesium (Mg) atoms; thus, the energy level of atomic oxygen is located below that of atomic Mg. As cations and anions assemble to build a solid MgO structure, it is expected that the energy of bonding orbitals, representing mainly oxygen p-orbitals, will decrease, and that of the antibonding orbitals, composed mainly of magnesium s-orbitals, will increase. In the case of oxygen vacancies, magnesium atoms with dangling bonds remain near their atomic energy levels, not increasing their energy through the interaction with oxygen atoms; thus, the band gap width decreases and yields narrower band gaps compared with the structures without oxygen vacancy.

To examine how the defects densities are affected by the presence of oxygen, the samples were heated at 600 °C in the vacuum chamber for 30, 60, and 90 min.

We measured the surface states and energy band gaps in the heated MgO material by using XPS and HR-REELS.

XPS and HR-REELS spectra were obtained by using the VG ESCALAB 210 and MICROLAB 350 apparatuses. XPS measurements used an Mg source with pass energy of 20 eV. The incidence and takeoff angles of electrons were 55° and 0°, respectively, relative to the surface normal. The binding energies were referenced to the C1 s peak of hydrocarbon contaminants at 285 eV.

Figures 3(a), 3(b) and 3(c) show the XPS spectral peaks of C1s, O2p, and Mg 2p, for heating at 600 °C, for different durations of 30, 60, and 90 min, respectively.

Usually, the MgO surface is contaminated by $H_2O$ and $CO_2$, with the as received status as shown in Fig. 3. Figure 3(a) shows the presence of two carbon peaks at the C1s core level. The first peak, located at 285.0 eV, is associated with the presence of residual C-C/CH groups (adventitious by hydrocarbon contamination).[28] At 290 eV, another peak is observed, corresponding to $CO_2$ carbonate,[4] and the $CO_2$ peak decreases with longer heating time. Similarly, as shown in Figs. 3(b) and 3(c), the $Mg(OH)_2$ and $OH/H_2O$ peaks decreased as the heating time increased. As a result, the MgO surface was contaminated by $H_2O$ and $CO_2$. Many additional oxygen atoms exist and they introduce defect states. When the sample was heated in vacuum, the adsorbed $H_2O$ and $CO_2$ were desorbed.

In addition, by increasing the annealing time, the amount of oxygen was reduced, increasing the oxygen vacancy (Table I).

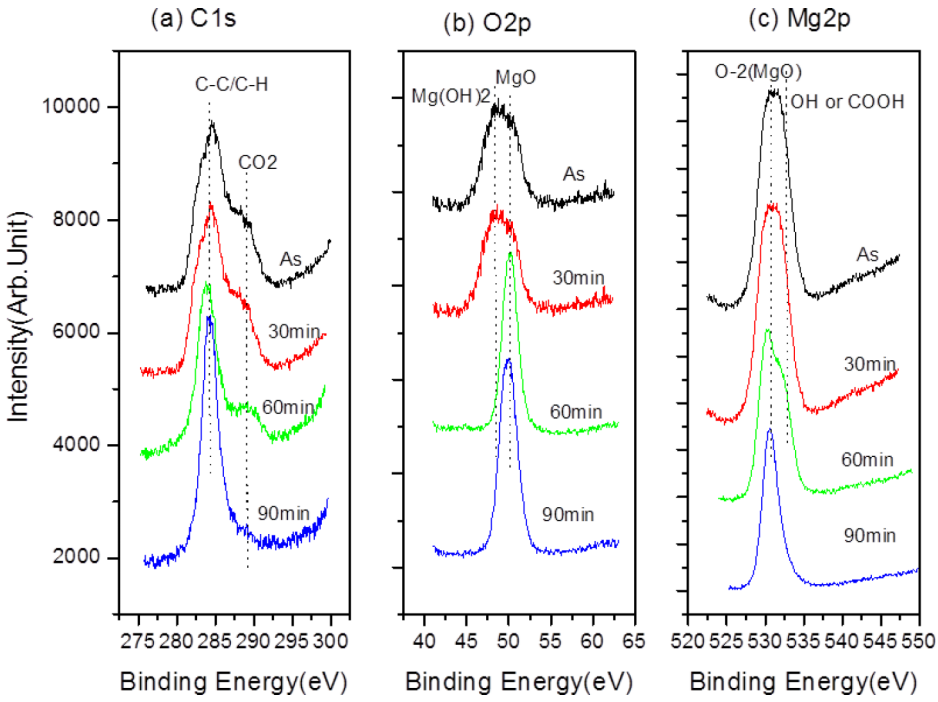


FIG. 3. (a), (b), (c) XPS spectra with C1s, O2p and Mg2p peaks, respectively, for various heating times (as, 30, 60, 90 min) at 600 °C, respectively.

Figure 4 shows the HR-REELS spectra for various heating times at 600 °C. The heights of the 4.2 eV and 6.3 eV peaks of REELS increased as the heating time increased (Fig. 4). From the previous results in Fig. 2 and Fig. 4, we confirmed that the $F_S$ center peak increased with decreasing oxygen on the surface of the MgO thin film.

Figure 5 shows the density of states (DOS) for $F_S$ centers containing oxygen vacancies of 3%, 6%, and 11% at the surface. Based on this result, when the oxygen vacancy increased by 3%, 6%, and 11%, the $F_S$ center peaks also increased and became broader.

A schematic of the energy diagram for Xe+ ion-initiated secondary electron emission via Auger neutralization process from the MgO surface is shown in Fig. 6. As an ion with an ionization energy (Ei) approaches the MgO surface, it undergoes the Auger neutralization process. In this process, one electron with energy E1 in the valance band of MgO is captured by the ion. When the released energy of Ei- $\chi$- $E_g^S$ is transferred to another valence electron, and the energy of the excited electron exceeds the vacuum level, the electron escapes from the surface as a secondary electron, with typical $E_g^S$ and electron affinity $\chi$ values of 6.3 and 0.85-1.0 eV, respectively.[29] In the case of Xe+ irradiation onto a defect-free MgO surface (Fig. 6(a)), because the difference between the energies of a valence electron in the MgO and the ionized shell in an Xe+ ion is lower than that required for secondary electron emission, the secondary electron will not be emitted at all. By contrast, secondary electron emission from the MgO surface via the Auger neutralization process

TABLE I. Composition of Mg to O by using X-ray photoelectron spectroscopy (XPS).

| Annealing Time | Mg | O | O/Mg |
|---|---|---|---|
| As dep. | 38.2 | 56.3 | 1.47 |
| 30 min | 43.9 | 54.9 | 1.25 |
| 60 min | 45.5 | 53.3 | 1.17 |
| 90 min | 47.8 | 51.1 | 1.07 |

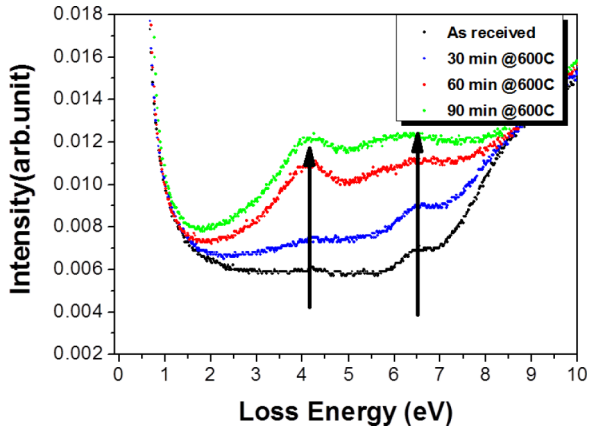


FIG. 4. HR-EELS spectra for MgO films at a primary beam energy of 0.3 keV, for various heating times (as, 30 min, 60 min, 90 min) at 600 °C.

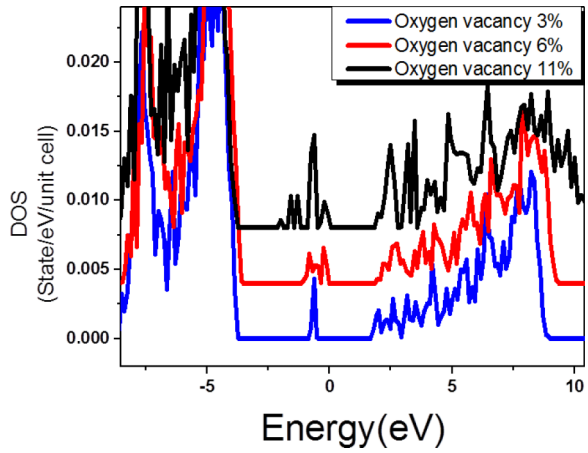


FIG. 5. Density of states (DOS) for $F_S$ centers containing oxygen vacancies of 3%, 6%, and 11 at% at the surface.

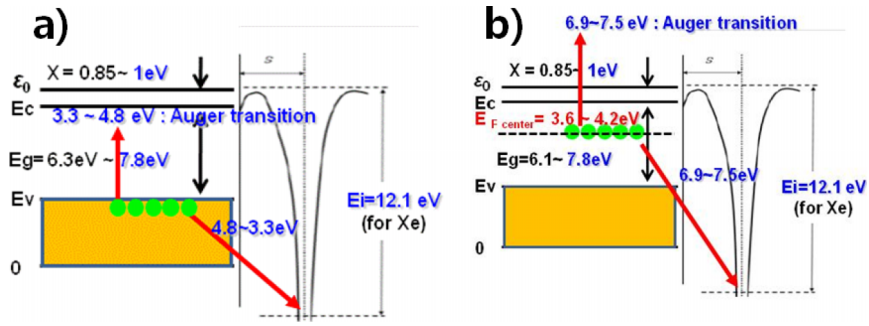


FIG. 6. Schematic of the Auger transition of an ion at an MgO surface (e.g. for Xe), which has the surface and bulk F center (a) without defect states and (b) with defect states.

under Xe+ irradiation is energetically permitted only when the surface has defect states (Fig. 6(b)). Therefore, the secondary electron yield increases with increasing the defects density.

The secondary electron emission yield ($\gamma$) is calculated from the following formula, developed by Motoyama *et al.*,[30]

$$,\gamma = \int_{\max\{E_i-\varepsilon_0,\ \varepsilon_0\}}^{E_i-2\xi+\varepsilon_0} P_e(\varepsilon)\, D_c(\varepsilon)\, T\left[\frac{\varepsilon+\varepsilon_0-E_i}{2}\right] d\varepsilon \Big/ \int_{\max\{E_i-\varepsilon_0,\ \varepsilon_c\}}^{E_i-2\xi+\varepsilon_0} D_c(\varepsilon)\, T\left[\frac{\varepsilon+\varepsilon_0-E_i}{2}\right] d\varepsilon \quad (1)$$

TABLE II. Calculated γ values based on the Auger transition between the valance band and $F_S$ centers with 3%, 6% and 11% oxygen vacancies. The ionization energies in eV are given in parentheses for each noble gas.

| | Perfect surface Mg(100) | 3% Oxygen vacancy | 6% Oxygen vacancy | 11% Oxygen vacancy |
|---|---|---|---|---|
| Work function (eV) | 7.110 | 4.544 | 4.384 | 4.284 |
| He (24.58) | 0.377 | 0.359 | 0.354 | 0.342 |
| Ne (21.56) | 0.351 | 0.332 | 0.318 | 0.303 |
| Ar (15.76) | 0.091 | 0.168 | 0.210 | 0.224 |
| Kr (14.00) | 0.000 | 0.083 | 0.175 | 0.193 |
| Xe (12.13) | 0.000 | 0.022 | 0.050 | 0.063 |

where $\varepsilon_0$ and $\varepsilon_c$ are the vacuum level and the conduction band minimum measured from the valence band bottom, respectively. $\xi$ is the work function given as a sum of the band gap and electron affinity for insulators. $D_c(\varepsilon)$ is the density of states for the conduction bands. $P_e$ and T describe the escape probability and the Auger transformation of the density of states, respectively. $P_e$ is given as follows:

$$P_e(\varepsilon) = \frac{1}{2}[1 - \frac{\varepsilon_0{}^{\beta}}{\varepsilon}]^{\alpha} \tag{2}$$

where $\alpha$ and $\beta$ are adjustable parameters with $\alpha = 0.248$ and $\beta = 1.0$.[7] The Auger transform is

$$T\left[\frac{\varepsilon + \varepsilon_0 - E_i}{2}\right] = \int_0^{\varepsilon_v}\int_0^{\varepsilon_v} D_v(\varepsilon_1) D_v(\varepsilon_2) \times \delta(\varepsilon - \varepsilon_1 - \varepsilon_2 + \varepsilon_0 - E_i)d\varepsilon_1 d\varepsilon_2 \tag{3}$$

where $\varepsilon_v$ and $D_v(\varepsilon)$ are the valence top energy and density of states for the valance band, respectively. The delta function allows electronic transitions that satisfy the energy conservation law. The $\varepsilon_0$, $\varepsilon_c$, $\xi$, and $D_c(\varepsilon)$ were obtained by first-principles calculation mentioned above. We confirmed that our calculations, using the hybrid functional approach, yielded accurate parameters, because those parameters are closely related to band gap and band structures. Details of the calculation can be found in Ref. 25.

The computed γ values for the surface with oxygen vacancy are listed in Table II. For a perfect MgO(100) surface, the value of γ under Kr+ and Xe+ irradiation is zero, as expected, indicating that the existence of defect states is required for secondary electron emission from the MgO surface under Kr+ and Xe+ irradiation. γ increased with increasing oxygen vacancy. On the other hand, in the case of He+ and Ne+ irradiation, γ tended to decrease with increasing oxygen vacancy.

In the cases of Kr+ and Xe+, for which the ionization energies are low, γ does not exist in the case of perfect MgO. The probability that the electrons in the valance band are elevated to the vacuum level is zero, as shown in Fig. 6(a).

When oxygen vacancies are present, the electrons that are trapped in the defect states jump to the vacuum level, increasing the value of γ, causing a stronger dependency on the defect states, as shown in Fig. 6(b).

In the case of He+ and Ne+, however, γ is large. We infer that He+ and Ne+ are not influenced by the defect states owing to their higher ionization energies. On the other hand, Ar+, Kr+, and Xe+ have small ionization energies, leading to a stronger dependency of γ on the defect states.

## IV. CONCLUSION

We measured the band gap energy and the energy level of defect states in MgO thin films by HR-REELS and REELS, and demonstrated the energy states of surface F centers in the MgO films. Our results demonstrate that HR-REELS peaks correspond to surface F centers ($F_S$) induced by oxygen vacancies. The HR-REELS peak height increases as the number of oxygen vacancies increases. The surface F center was experimentally measured and confirmed through a first-principles calculation.

We found that He+ and Ne+ were not influenced by the defect states owing to their higher ionization energies; however, Ar+, Kr+ and Xe+ led to a stronger dependency of γ on the defect states owing to their small ionization energies.


[1] E.H. Choi, H.J. Oh, Y.G. Kim, J.J. Ko, J.Y. Lim, J.G. Kim, D.I. Kim, G.S. Cho, and S.O. Kang, Jpn. J. Appl. Phys. **37**, 7015 (1998).
[2] S.J. Yoon, I.S. Lee, J.W. Lee, and B.D. Oh, Jpn. J. Appl. Phys. **40**, 809 (2001).
[3] T. Nagatomi, T. Kuwayama, Y. Takai, K. Yoshino, Y. Morita, M. Kitagawa, and M. Nishitani, Appl. Phys. Lett. **92**, 084104 (2008).
[4] T. Nagatomi, T. Kuwayama, K. Yoshino, Y. Takai, Y. Morita, M. Nishitani, and M. Kitagawa, J. Appl. Phys. **106**, 104912 (2009).
[5] T. Ugrade, T. Iemori, M. Osawa, N. Nakayama, and I. Morita, IEEE Trans. Electron Devices **23**, 313 (1976).
[6] H.D. Hagstrum, Phys.Rev. **96**, 336 (1954).
[7] T. Tsujita, T. Nagatomi, and Y. Takai, Surf. Interface Anal. **37**, 137 (2005).
[8] T. Tsujita, K. Nakayama, T. Nagatomi, Y. Takai, Y. Morita, M. Nishitani, M. Kitagaa, and T. Uenoyama, J. Surf. Anal. **12**, 284 (2005).
[9] T. Nagatomi, T. Kuwayama, Y. Takai, K. Yoshino, Y. Morita, M. Kitagawa, and M. Nishitani, Appl. Phys. Lett. **92**, 084104 (2008).
[10] T. Nagatomi, T. Kuwayama, K. Yoshino, Y. Takai, Y. Morita, M. Nishitani, and M. Kitagawa, J. Appl. Phys. **106**, 104912 (2009).
[11] K. Yoshino, T. Nagatomi, Y. Morita, T. Oue, N. Kosugi, M. Nishitani, M. Kitagawa, and Y. Takai, Jpn. J. Appl. Phys. **49**, 086205 (2010).
[12] K. Yoshino, T. Nagatomi, Y. Morita, T. Oue, N. Kosugi, M. Nishitani, M. Kitagawa, and Y. Takai, Jpn. J. Appl. Phys. **49**, 040212 (2010).
[13] K. Yoshino, T. Nagatomi, Y. Morita, T. Oue, N. Kosugi, M. Nishitani, M. Kitagawa, and Y. Takai, Jpn. J. Appl. Phys. **50**, 026201 (2011).
[14] K. Yoshino, Y. Morita, T. Nagatomi, M. Terauchi, T. Tsujita, T. Nakayama, Y. Yamauchi, M. Nishitani, M. Kitagawa, Y. Yamauchi, and Y. Takai, J. Surf. Anal. **18**, 13-25 (2011).
[15] K. Yoshino, Y. Morita, T. Nagatomi, M. Terauchi, T. Tsujita, Y. Doi, T. Nakayama, Y. Yamauchi, M. Nishitani, M. Kitagawa, Y. Yamauchi, and Y. Takai, Appl. Surf. Sci. **259**, 135 (2012).
[16] Y. Motoyama, Y. Hirano, K. Ishii, Y. Murakami, and F. Sato, J. Appl. Phys. **95**, 8419 (2004).
[17] G.H. Rosenblatt, M.W. Rowe, G.P. Williams, Jr., and R.T. Williams, Phys. Rev. B **39**, 10309 (1989).
[18] R. I. Eglitis, M. M. Kuklja, E. A. Kotomin, A. Stashans, and A. I. Popov, Comp. Mat. Sci. **5**, 298 (1996).
[19] M.C. Wu, C.M. Truong, and D.W. Goodman, Phys. Rev. B **46**, 2688 (1992).
[20] H. Jin, S. K. Oh, H. J. Kang, and M.H. Cho, Appl. Phys. Lett. **89**, 122901 (2006).
[21] S. Tanuma, C. J. Powell, and D. R. Penn, Surf. Interf. Anal. **21**, 165 (1994).
[22] D. M. Roessler and W. C. Walker, Phys. Rev. **159**, 733 (1967).
[23] V.E. Henrich *et al.*, Phys.Review B **22**, 4764 (1980).
[24] K.P. McKenna and A.L. Shluger, Phy.Rev. B **79**, 224116 (2009).
[25] Y. Cho, C. Kim, H.S. Ahn, E. Cho, T.E. Kim, and S. Han, J. Appl. Phys. **101**, 083710 (2007).
[26] D. Bagayoko, AIP Advances **4**, 127104 (2014).
[27] M. Dadsetani and R. Beiranvand, Solid State Science **11**, 2099 (2009).
[28] S Feliu, Jr. and ML Perez-Revenga, Met Mater Trans A **35A**, 2039 (2004).
[29] M.O. Aboelfotoh and J.A. Lorenzen, J.Appl.Phys. **48**, 4754 (1997).
[30] Y. Motoyama, H. Matsuzaki, and H. Murakami, IEEE Trans. Electron Devices **48**, 1568 (2001).